levels[4]. Our analysis shows that it is appropriate and necessary to attempt restoration on a global scale, and provides a benchmark against which community recovery could be assessed. □

Methods

Data selection

For shelf communities, we compiled data from research trawl surveys from the Southern Grand Banks (43–46° N, 49–53° W) and Saint Pierre Banks (45–47° N, 55–58° W) (ref. 28), the Gulf of Thailand (9–14° N, 100–105° W) (ref. 29) and South Georgia (53–56° S, 35–40° W) (ref. 14). All other trawl data sets that we considered (for example, North Sea, Georges Bank and Alaska) did not capture the beginning of industrialized exploitation. We included only demersal predators; pelagic species, which were not well sampled by the trawl gear, were excluded. Longlining data obtained from the Japanese Fishery Agency were divided into temperate (Atlantic, 40–45° S; Indian, 35–45° S; Pacific, 30–45° S), subtropical (Atlantic, 10–40° S; Indian, 10–35° S; Pacific, 15–30° S) and tropical communities (Atlantic, 20° N–10° S; Indian, 15° N–15° S; Pacific, 10–15° S). These divisions were based on their dominant species: yellowfin (*T. albacares*), albacore (*T. alalunga*) or southern bluefin tuna (*T. maccoyii*), respectively, and excluded areas previously fished by the Japanese, Spanish and US fleets. Running the models with alternative divisions (±5°) did not change the results significantly. The catch rates in each community were determined as the sum of the catches divided by the sum of the effort in each region in each year. Years with very low effort (<20,000 hooks for the entire region) were excluded. Alternative treatment of the data, including removing seasonal effects and taking the average catch rates over 5° × 5° squares, had little effect on the results. For longlines, we assume that the catch rate is an approximate measure of relative biomass, which is probably conservative because the average individual weights of fish in exploited populations tend to decline over time. Our data capture the abundance of larger fishes that are vulnerable to baited hooks and bottom trawls, respectively. Many smaller species have low catchabilities and are not recorded reliably by these methods. Changes in the longline fishery occurred around 1980 when the fishery began to expand into deeper regions; however, this was only after the declines in biomass were observed. For more details on species composition, data treatment and interpretation of trends, refer to the Supplementary Information.

Data analysis

Our model (equation (1)) assumes that for each community, i, the rate of decline to equilibrium is exponential with rate r_i from a pre-exploitation biomass $N_i(0)$, where $t = 0$ is the first year of industrialized fishing. Exploitation continues until equilibrium is approached, where a residual proportion, δ_i, of the biomass remains. We fit this model separately to each community under the assumption of a lognormal error distribution using nonlinear regression (Procedure NLIN in SAS, version 8). We also used nonlinear mixed-effects models[13] to determine whether the patterns were similar across communities. Mixed-effect models were fitted by maximizing the likelihood integrated over the random effects using adaptive gaussian quadrature (Procedure NLMIXED in SAS). To account for the fact that biomass was recorded in different units (kilotonnes (kt), catch rates), the initial biomass, $N_i(0)$, was assumed to be a fixed effect for each community with appropriate units. For South Georgia, $N_i(0)$ was fixed at the first biomass estimate to capture the high initial rate of decline. This first estimate (750 kt; ref. 14) was considered to be realistic because it was very close to the sum of total removals (514 kt; ref. 30) plus the residual biomass estimate (160 kt; ref. 14) after the first 2 years of fishing. Autocorrelation in the residuals of some time series may cause the standard errors to be underestimated. The results were robust to alternative error assumptions (separate error variances for the time series and alternative error distributions); for example, under the assumption of normal errors, the rate of decline was 13.9% and residual biomass was 10.9%, respectively.

Received 25 November 2002; accepted 25 March 2003; doi:10.1038/nature01610.

1. Pauly, D. & Christensen, V. Primary production required to sustain global fisheries. *Nature* **374,** 255–257 (1995).
2. Tegner, M. J. & Dayton, P. K. Ecosystem effects of fishing. *Trends Ecol. Evol.* **14,** 261–262 (1999).
3. Pauly, D. *et al.* Towards sustainability in world fisheries. *Nature* **418,** 689–695 (2002).
4. United Nations. *World Summit on Sustainable Development: Plan of Implementation* ⟨http://www.johannanesburgsummit.org/html/documents/summit_docs/2309_planfinal.htm⟩ (United Nations, New York, 2002).
5. Jackson, J. B. C. *et al.* Historical overfishing and the recent collapse of coastal ecosystems. *Science* **293,** 629–638 (2001).
6. Steele, J. H. & Schumacher, M. Ecosystem structure before fishing. *Fish. Res.* **44,** 201–205 (2000).
7. Worm, B., Lotze, H. K., Hillebrand, H. & Sommer, U. Consumer versus resource control of species diversity and ecosystem functioning. *Nature* **417,** 848–851 (2002).
8. Pauly, D. Anecdotes and the shifting baseline syndrome of fisheries. *Trends Ecol. Evol.* **10,** 430 (1995).
9. Field, C. B., Behrenfeld, M. J., Randerson, J. T. & Falkowski, P. Primary production of the biosphere: integrating terrestrial and oceanic components. *Science* **281,** 237–240 (1998).
10. Myers, R. A., Hutchings, J. A. & Barrowman, N. J. Why do fish stocks collapse? The example of cod in Atlantic Canada. *Ecol. Appl.* **7,** 91–106 (1997).
11. Bullis, H. R. Preliminary report on exploratory longline fishing for tuna in the Gulf of Mexico and the Caribbean Sea. *Comm. Fish. Rev.* **17,** 1–15 (1955).
12. Shomura, R. S. & Murphy, G. I. *Longline Fishery for Deep-Swimming Tunas in the Central Pacific, 1953.* US Fish and Wildlife Service Special Scientific Report: Fisheries No. 157 (USFWS, Washington, 1955).
13. Davidian, M. & Giltinan, D. M. *Nonlinear Models for Repeated Measurement Data* (Chapman & Hall, New York, 1995).
14. Kock, K.-H. & Shimadzu, Y. in *Southern Ocean Ecology: The BIOMASS Perspective* (ed. El-Sayed, S. Z.) 287–312 (Cambridge Univ. Press, Cambridge, 1994).
15. Hutchings, J. A. & Myers, R. A. in *The North Atlantic Fisheries: Successes, Failures and Challenges* (eds Arnason, R. & Felt, L.) 38–93 (The Institute of Island Studies, Charlottetown, Prince Edward Island, Canada, 1995).
16. Rothschild, B. J. Competition for gear in a multiple-species fishery. *J. Cons. Int. Explor. Mer.* **31,** 102–110 (1967).
17. Lyne, V., Parslow, J., Young, J., Pearce, A. & Lynch, M. *Development, Application and Evaluation of the Use of Remote Sensing Data by Australian Fisheries* (CSIRO Marine Research, Hobart, Australia, 2000).
18. Caton, A. E. A review of aspects of southern bluefin tuna biology, population and fisheries. *Inter-Am. Trop. Tuna Comm. Spec. Rep.* **7,** 181–350 (1991).
19. Stevens, J. D., Bonfil, R., Dulvy, N. K. & Walker, P. A. The effects of fishing on sharks, rays, and chimaeras (chondrichthyans), and the implications for marine ecosystems. *ICES J. Mar. Sci.* **57,** 476–494 (2000).
20. Baum, J. K. *et al.* Collapse and conservation of shark populations in the Northwest Atlantic. *Science* **299,** 389–392 (2003).
21. Fogarty, M. J. & Murawski, S. A. Large-scale disturbance and the structure of marine systems: Fishery impacts on Georges Bank. *Ecol. Appl.* **8** (suppl.), 6–22 (1998).
22. Watson, R. & Pauly, D. Systematic distortions in world fisheries catch trends. *Nature* **414,** 534–536 (2001).
23. Pauly, D., Christensen, V., Dalsgaard, J., Froese, R. & Torres, F. Jr Fishing down marine food webs. *Science* **279,** 860–863 (1998).
24. Roberts, C. M. Deep impact: the rising toll of fishing in the deep sea. *Trends Ecol. Evol.* **242,** 242–245 (2002).
25. Worm, B. & Myers, R. A. Meta-analysis of cod–shrimp interactions reveals top–down control in oceanic food webs. *Ecology* **84,** 162–173 (2003).
26. Myers, R. A. & Mertz, G. The limits of exploitation: a precautionary approach. *Ecol. Appl.* **8** (suppl.), 165–169 (1998).
27. Casey, J. M. & Myers, R. A. Near extinction of a large, widely distributed fish. *Science* **281,** 690–692 (1998).
28. Casey, J. M. *Fish Assemblages on the Grand Banks of Newfoundland*. Thesis, Memorial Univ. Newfoundland, Canada (2000).
29. Pauly, D. in *Fish Population Dynamics* (ed. Gulland, J. A.) 329–348 (Wiley, New York, 1988).
30. Commission for the Conservation of Antarctic Marine Living Resources *Statistical Bulletin* Vol. 14 (CCAMLR, Hobart, Australia, 2002).

Supplementary Information accompanies the paper on **www.nature.com/nature**.

Acknowledgements We thank J. Casey, A. Fonteneau, S. Hall, J. Hampton, S. Harley, J. Ianelli, I. Jonsen, J. Kitchell, K.-H. Kock, H. Lotze, M. Maunder, T. Nishida, M. Prager, T. Quinn, G. Scott and P. Ward for data, comments and suggestions, N. Barrowman and W. Blanchard for statistical advice, and D. Swan for technical assistance. This research is part of a larger project on pelagic longlining initiated and supported by the Pew Charitable Trusts. Further support was provided by the Deutsche Forschungsgemeinschaft and the National Sciences and Engineering Research Council of Canada.

Competing interests statement The authors declare that they have no competing financial interests.

Correspondence and requests for materials should be addressed to R.A.M. (Ransom.Myers@dal.ca).

Attractor dynamics of network UP states in the neocortex

Rosa Cossart, Dmitriy Aronov & Rafael Yuste

Department of Biological Sciences, Columbia University, New York, New York 10027, USA

The cerebral cortex receives input from lower brain regions, and its function is traditionally considered to be processing that input through successive stages to reach an appropriate output[1,2]. However, the cortical circuit contains many interconnections, including those feeding back from higher centres[3–6], and is continuously active even in the absence of sensory inputs[7–9]. Such spontaneous firing has a structure that reflects the coordinated activity of specific groups of neurons[10–12]. Moreover, the membrane potential of cortical neurons fluctuates spontaneously between a resting (DOWN) and a depolarized (UP) state[11,13–16], which may also be coordinated. The elevated firing rate in the UP state follows sensory stimulation[16] and provides a substrate for

persistent activity, a network state that might mediate working memory[17–21]. Using two-photon calcium imaging, we reconstructed the dynamics of spontaneous activity of up to 1,400 neurons in slices of mouse visual cortex. Here we report the occurrence of synchronized UP state transitions ('cortical flashes') that occur in spatially organized ensembles involving small numbers of neurons. Because of their stereotyped spatiotemporal dynamics, we conclude that network UP states are circuit attractors—emergent features of feedback neural networks[22] that could implement memory states or solutions to computational problems.

To investigate the spatiotemporal dynamics and mechanisms of persistent neocortical activity, we used two-photon calcium imaging to reconstruct the spontaneous activity of large neuronal populations with single-cell resolution (184–1,396 cells, 650 on average; Fig. 1). Unstimulated neocortical slices perfused with standard artificial cerebrospinal fluid (aCSF) always exhibited persistent spontaneous activity, as detected by imaging spontaneous calcium transients[12] (Fig. 1c). All calcium transients were blocked by the bath application of the sodium channel blocker tetrodotoxin (1 μM, $n = 14$; not shown) or voltage-sensitive calcium channel (VSCC) antagonists (2 mM Ni^{2+} or 200 μM Cd^{2+}, $n = 13$; not shown). As in our previous work[12], we concluded that calcium transients were due to the opening of somatic VSCCs by sodium action potentials, and that they could be used as an indicator that action potentials had occurred in a given cell.

To analyse the spontaneous activity of the entire network, we measured fluorescence changes in each cell and recorded the peak time of each calcium transient (Fig. 1c; see Methods). We then combined calcium transients from all cells into rasterplots and collapsed these rasterplots into activity histograms, which indicated the percentage of active cells as a function of time (Fig. 1d). On average, 0.4 ± 0.1% of cells were active within any given 1-s interval ($n = 168$ movies). In 78% of movies, these time histograms showed prominent peaks of synchronous activity (Fig. 1d, asterisks). Cells that were coactive during peaks of synchrony constituted a low, but significant, fraction of all imaged cells (2.2 ± 0.1%, $n = 414$). This is a considerably smaller fraction of cells than that active during other synchronous network phenomena in slices, such as epileptiform[23] or oscillatory[11] events. Furthermore, forms of persistent activity previously reported *in vitro* in modified slice media, or *in vivo*, were paroxysmal and propagative events that recruit most neurons[10,11,13–15]. Also, peaks of synchrony had no apparent periodicity and occurred with an average interval of 55 ± 4 s ($n = 249$ intervals), considerably less often than both epileptiform events (~1 Hz) and slow oscillations (0.1–0.5 Hz). Thus, the synchronizations we describe represent a different type of spontaneous event.

Synchronized neuronal ensembles were often spatially structured (Fig. 2; see Methods). At peaks of synchrony, coactive cells were either distributed across the imaged field (74% of peaks) or organized into clusters (19%), layers (4%) or columns (3%). Clusters were found in layers II/III or V, whereas layers and columns could involve any layer. Interestingly, many peaks of synchronous activity were preceded by a gradual build-up and followed by a gradual decrease in the number of active cells. In some cases, a significant fraction of cells was active up to 5 s before and after the peak of synchrony (Fig. 3A). In addition, the spatial arrangement of coactive cells gradually became organized during the period of time preceding the peak (Fig. 3B). Even 5 s away from the peaks, 13% of

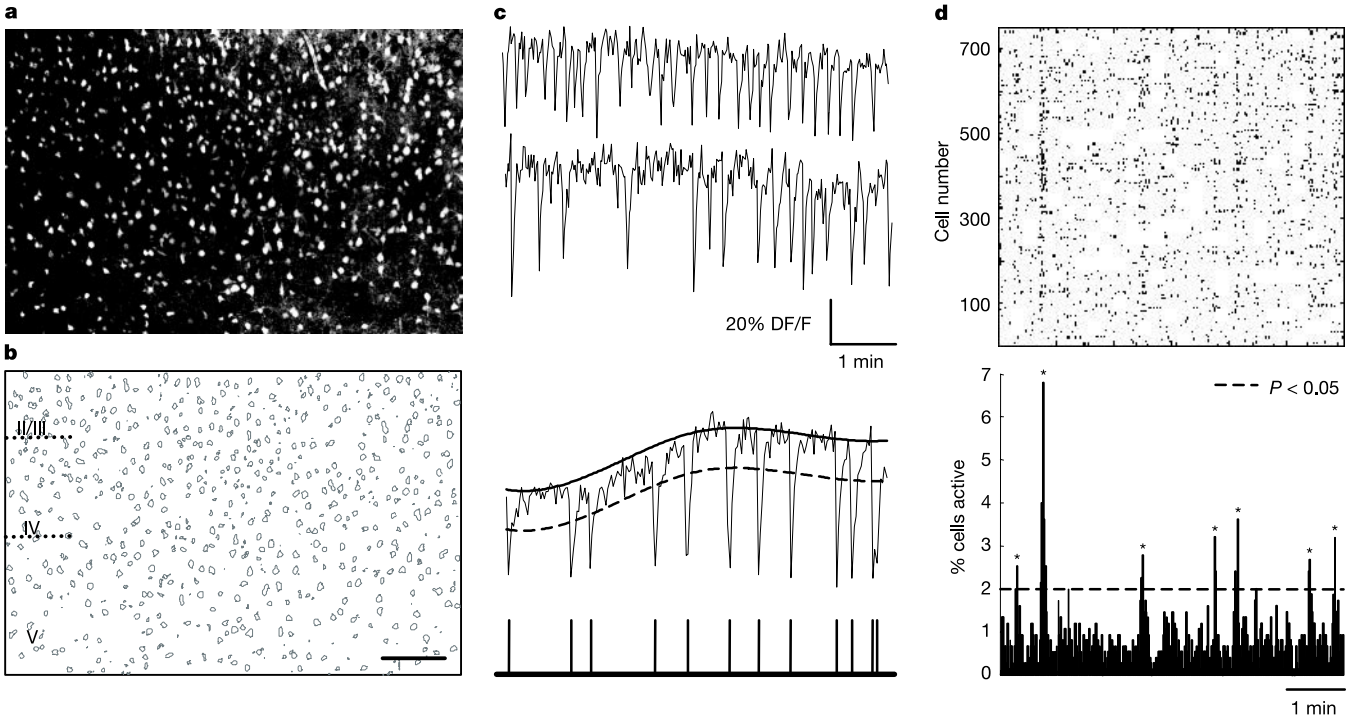

Figure 1 Two-photon calcium imaging of persistent activity in large neuronal populations. **a**, Two-photon calcium-fluorescence image taken at low magnification (× 20) of a slice from area V1. The image is an average of 300 consecutive frames. Time resolution, 1.2 s per frame. For a sample movie, see Supplementary Information. **b**, Contours of the 754 cells from the fluorescence image were detected by an automatic procedure. Scale bar, 100 μm. **c**, Top: representative traces of calcium transients. Time resolution, 1.2 s per frame. Bottom: example of calcium-transient detection. **d**, Top: representative rasterplot in which each row represents a single cell, and each mark a detected calcium transient. Bottom: histogram representing the percentage of cells active at each frame of the movie. Asterisks mark significant peaks of synchrony. Time resolution, 1.2 s per frame.

the patterns were found to be in one of the spatially stereotyped categories (clusters, layers or columns). This percentage increased gradually to 24% throughout the duration of the onset, and decreased gradually throughout the duration of the offset of the events ($n = 228$ events; not shown). Thus, the peaks of synchronous activity corresponded to maximal spatial organization of the coactive cells.

In most movies, more than one peak of synchronous activity was detected, and some cells were repeatedly active at several peaks (Fig. 3A). Specifically, 17% of the spatial patterns of coactive cells had a significant overlap ($P < 0.05$) with at least one other pattern at a peak of synchrony ($n = 228$ events). On average, 4.9 ± 0.1% of the coactive cells were repeatedly coactive at another peak. The overlap was more pronounced (30% of peaks, 9.5 ± 0.2% of cells) when cells active throughout the entire duration of the events were included. Thus, not only the neurons active at peaks of synchrony, but also the temporal sequences of coactive groups immediately before and after the peaks, tended to be significantly repetitive. We conclude that the spontaneous coactivations can repeatedly involve the same components of the network, following similar dynamical trajectories.

We investigated the physiological events responsible for the described patterns of activity by targeting cells active at peaks of synchrony online and performing current-clamp recordings (Fig. 4). Cells were also filled with biocytin and could thus be morphologically identified post hoc. Most cells active at peaks (71%, $n = 17$) were pyramidal neurons, whereas the rest ($n = 5$) were interneurons. Surprisingly, electrophysiological recordings revealed that the membrane potential of most coactive cells (96%, $n = 50$) fluctuated between two states (Fig. 4). This property was not observed in randomly patched cells ($n = 10$). UP and DOWN membrane potential states were −56 ± 1 mV and −65 ± 1 mV, respectively ($n = 33$). Durations of UP states ranged from about 60 ms to 30 s (Fig. 4B). Transitions to the UP state were fast and occurred within 58 ± 5 ms, whereas transitions to the DOWN state could be fitted by a single exponential function with a time constant of 164 ± 46 ms. In 55% of cases, the UP state was suprathreshold, with a firing frequency of 21 ± 9 Hz and an average of 12 ± 4 spikes per state ($n = 12$). Suprathreshold UP states always produced detectable calcium transients (see Methods). In 44% of the neurons that showed suprathreshold UP states, low-frequency firing also occurred in the DOWN state (0.64 ± 0.18 Hz, $n = 8$ cells). However, such firing could not be detected in the imaging. In several cases, a cell participated a second time in a peak after it was patched, enabling us to perform simultaneous electrical and optical recordings during a synchronous event. During peaks of synchrony, cells did indeed exhibit a shift of the membrane potential to a depolarized UP state with sustained high-frequency firing (Fig. 4A). Thus, we conclude that cells involved in peaks of synchrony exhibit bimodal membrane potentials, and that synchrony occurs when several neurons simultaneously shift to suprathreshold UP states, defining a coactive neuronal ensemble.

Finally, we investigated the cellular and synaptic mechanisms underlying the occurrence of the peaks of synchrony. The intracellular incidence of UP states in cells participating in network UP states in control conditions was almost entirely prevented by the AMPA (α-amino-3-hydroxy-5-methyl-4-isoxazole propionic acid)- and NMDA (*N*-methyl-D-aspartate)-receptor antagonists 2,3-dihydroxy-6-nitro-7-sulphamoylbenzo(*f*)quinoxaline (NBQX; 10 μM) and MK801 (10 μM), respectively (UP state frequency decreased by 93%, $n = 19$ cells; Fig. 4B). Surprisingly, in a few electrophysiological recordings in the presence of blockers of glutamatergic transmission, UP states still occurred, even when all excitatory postsynaptic potentials (EPSPs) were blocked ($n = 10$ cells; Fig. 4B). This indicates that glutamatergic transmission might not be essential for the generation of UP states in some cells. In these cells, all UP state transitions were blocked when GABA (γ-aminobutyric acid)-mediated transmission was suppressed by the further addition of picrotoxin (100 μM, $n = 8$ cells), an antagonist of $GABA_A$ receptors. Thus, we propose that UP states are synaptically

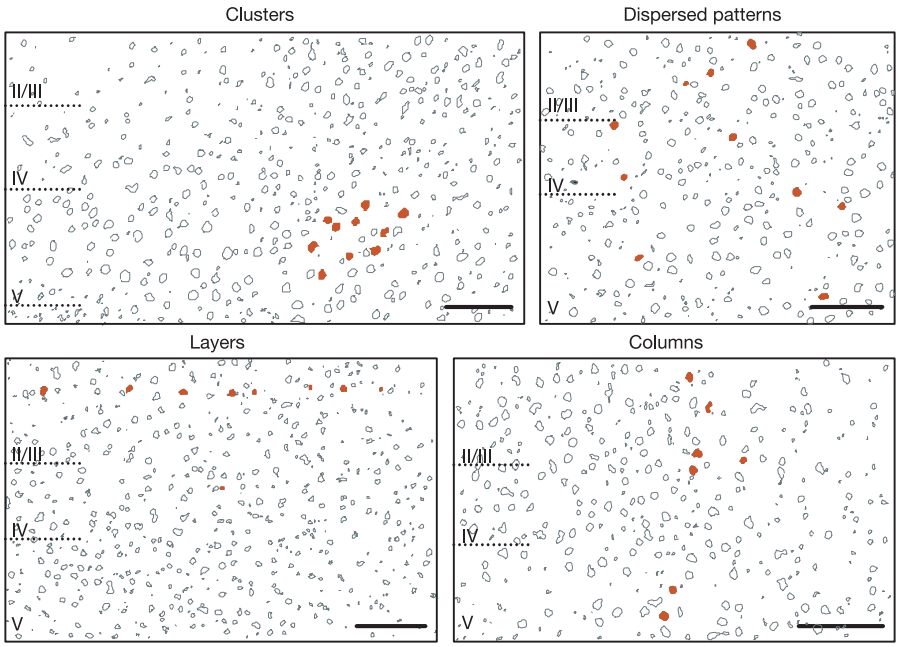

Figure 2 Spatial structure of synchronous neuronal ensembles. Representative contour plots of the four types of spatial arrangement of cells coactive at peaks of synchrony. Red contours indicate cells active at the movie frame corresponding to the peak of synchrony. Patterns were identified and classified using Monte Carlo simulations (see Methods). The dispersed pattern illustrated was detected in the movie provided in Supplementary Information. Scale bar, 100 μm.

driven by a combination of both glutamatergic and GABAergic transmission[24].

Two-photon calcium imaging of large neuronal populations, online reconstruction and analysis of individual signals, and intracellular recordings of targeted cells have enabled us to study the spatiotemporal dynamics of spontaneous cortical activity and to correlate it with intracellular responses. In the absence of any stimulation, networks in cortical slices exhibit characteristic patterns of synchronous activity. Coactivations occur during simultaneous transitions to membrane potential UP states. Coactive ensembles are often dispersed throughout different layers, but can be spatially organized in ways that reflect the underlying cortical architecture. The microcircuits of coactive cells participating in UP states are composed of small numbers of cells. Thus, these states differ from 'global' UP and DOWN states observed in other preparations[11,13,16], although the single-cell activity underlying them shares properties with the membrane fluctuations we report. Rather, the events we describe ('cortical flashes') are more reminiscent of the persistent activity states recorded in sparse populations of cells during working memory tasks in awake monkeys[17,18,25].

Intriguingly, the spontaneous peaks of synchrony studied here follow recurrent stereotyped spatiotemporal dynamics (Fig. 3). This seems to be analogous to the dynamical behaviour of feedback neural networks, which converge into 'attractors', theoretically defined as stable states in network dynamics[22]. These emergent stable states could represent the solution to a specific computation[22], and have been used to model orientation selectivity[26], eye position stability[21] and working memory[19,20].

Specifically, network UP states persist on timescales much longer than those of the feedforward information flow through the cortex[2], indicating that they are dynamically stable (Fig. 4). Furthermore, they represent repeatable patterns of coincident firing, often following dynamical trajectories involving the same subcircuits (Fig. 3). Thus, network UP states are unexpectedly probable, which implies that they are preferred states of the network. Hence, the build-up of synchrony that we image would correspond to the descent into an attractor basin (UP state). Finally, we observe a multiplicity of discrete patterns, where different collections of neurons are involved

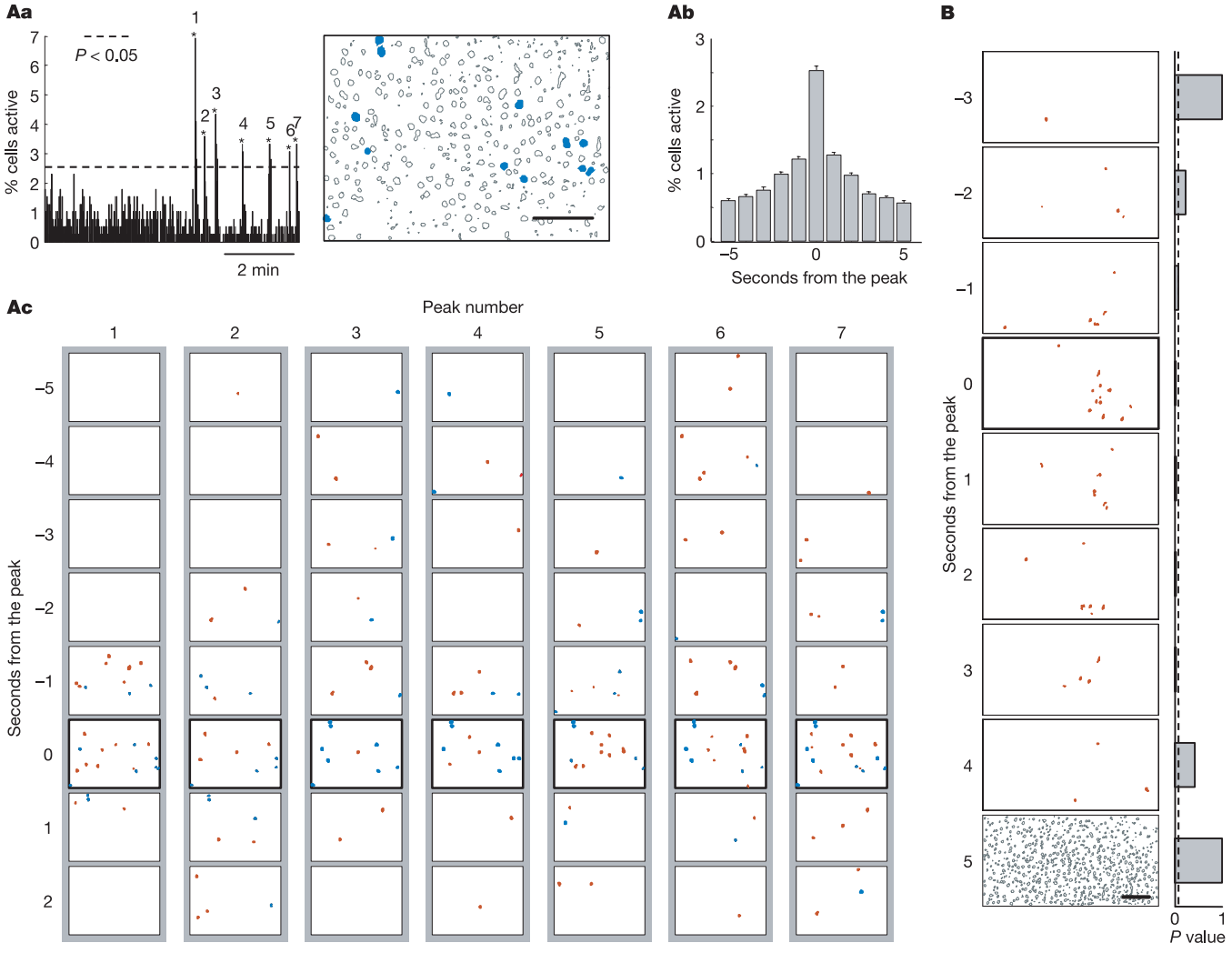

Figure 3 Spatiotemporal dynamics of synchronous activity. **Aa**, Repetitive activation of neuronal ensembles. Representative example showing multiple peaks of synchrony (asterisks). Blue contours indicate the cells repeatedly active at every peak. Time resolution, 1.1 s per frame. **Ab**, Average kinetics of peaks of synchrony from all movies ($n = 642$). **Ac**, Sequences of consecutive movie frames before and after each peak of synchrony (bold) in **Aa**. Only active cells are indicated. The cells active at every peak in **Aa** are indicated in blue. **B**, Frames of another movie before and after a peak of synchrony (0, bold). Red contours indicate active cells. All imaged cells are shown at frame 5. The bar graph indicates the significance of spatial organization. Scale bar, 100 μm.

in different patterns, and we find that single cells can be active in more than one of them, confirming theoretical predictions for attractor dynamics[22]. An alternative interpretation of our results is that we are imaging the activity of 'reporter neurons'; that is, postsynaptic cells driven in a feedforward fashion by 'hidden' attractor states. This possibility, however, still requires attractors to be present in the network.

We conclude that 'cortical flashes' are dynamical attractors, and that the isolated cortical microcircuit can not only generate them, but also produce a rich variety with specific and discrete anatomical patterns. Our data are consistent with the hypothesis that a principal function of the highly recurrent neocortical networks is to generate persistent activity that might represent mental states[3,7,27]. □

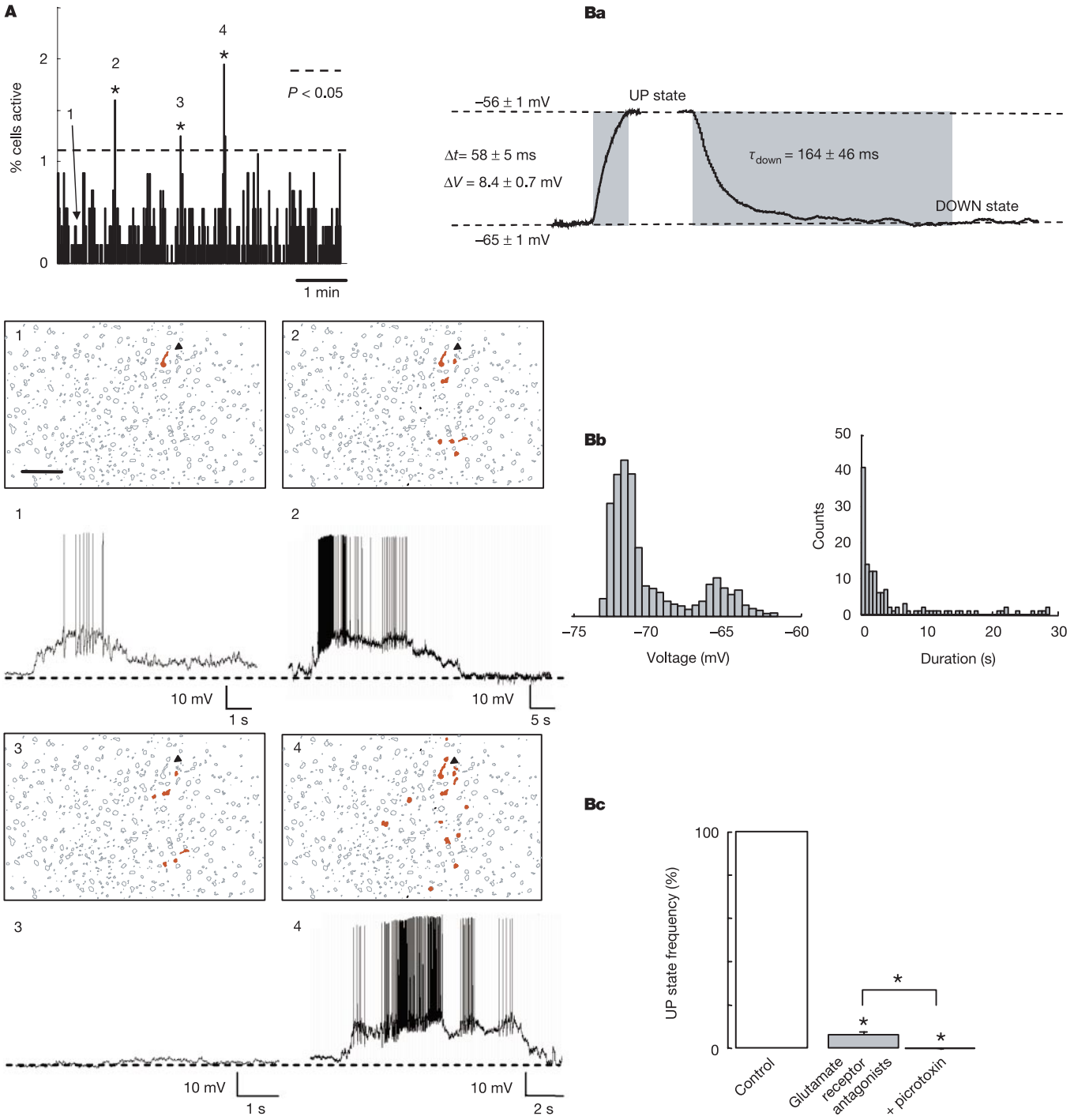

Figure 4 Synchronous activity is mediated by network UP states. **A**, Simultaneous imaging of network activity and current-clamp recording of a pyramidal cell (arrow) active at multiple peaks of synchrony (asterisks). Time resolution, 1.2 s per frame. Red contours indicate cells active at time points 1–4. Optical signals corresponded to shifts of the membrane potential to an UP state ($I = 0$ pA, $V_{down} = -70$ mV). Scale bar, 100 μm. **Ba**, Average kinetics of UP states ($n = 133$). Δt, length of onset; τ_{down}, time constant of average offset. **Bb**, Left: membrane potential distribution of a representative example. Right: distribution of UP state durations. **Bc**, Relative frequency of UP states in the presence of glutamatergic antagonists and after the further addition of the GABA receptor antagonist picrotoxin. Asterisks, $P < 0.05$.

Methods

Slice preparation and two-photon imaging

Slices (thickness, 300–350 μm) were prepared from visual cortices of P14-21 C57BL/6 mice using a Leica VT 1000S tissue slicer with ice-cold oxygenated modified aCSF that included 0.5 mM $CaCl_2$ and 7 mM $MgSO_4$, in which NaCl was replaced by an equimolar concentration of sucrose. For AM-loading, slices were incubated in a small vial containing 2.5 ml oxygenated aCSF with 25 μl 1 mM Fura2-AM solution (Molecular Probes; in 100% dimethylsulphoxide) for 20–30 min. Slices were incubated in the dark, and incubation solution maintained at 35–37 °C. Experiments were performed at 35–37 °C with aCSF containing (in mM) 123 NaCl, 3 KCl, 26 $NaHCO_3$, 1 NaH_2PO_4, 2 $CaCl_2$, 2 $MgSO_4$ and 10 dextrose, which was continuously aerated with 95% O_2, 5% CO_2. Imaging was carried out with a custom-made two-photon laser scanning microscope[28] consisting of a modified Fluoview (Olympus) confocal microscope with a Mira Ti:sapphire laser (Coherent) providing 130 fs pulses at 75 MHz, pumped by a solid-state source (Verdi, Coherent). Slices were imaged using a low-magnification, high-numerical-aperture objective (× 20, NA-0.95, Olympus). Frames were acquired at 0.9–1.6 s per frame. Size of the imaged field typically ~400 × 700 μm.

Electrophysiology

Cells were held in current clamp using a patch-clamp amplifier (BVC-700, Dagan Corporation). Pipette solution contained 130 mM potassium methylsulphate, 5 mM KCl, 5 mM NaCl, 10 mM HEPES, 2.5 mM Mg-ATP, 0.3 mM GTP, 30 μM Fura-2 pentapotassium salt (Molecular Probes) and 0.5% biocytin. The osmolarity was 265–275 mosM, pH 7.3. Microelectrodes had a resistance of 4–10 MΩ. Recordings were digitized online (10 kHz) with an A/D board (Instrutec) and analysed offline with MiniAnalysis 5.1 (Synaptosoft, Inc.). Neurons were filled with biocytin during recording and processed for morphological identification.

AMPA receptors were blocked by 6-cyano-7-nitroquinoxaline-2,3-dione (CNQX; 10 μM), 6,7-dinitro-2,3-quinoxalinedione (DNQX; 10 μM) or NBQX (10 μM). NMDA receptors were blocked by D-2-amino-5-phosphonopentanoate (AP5; 40 μM) or MK801 (10 μM). As we did not observe any significant differences in the effects of these antagonists, the data were pooled for further analysis. CNQX, DNQX, NBQX, picrotoxin and AP5 were purchased from Sigma; MK801 was obtained from Tocris.

Analysis

Online analysis was performed with custom-made software in ImageJ (National Institutes of Health) and Matlab (MathWorks). To detect calcium signals from imaged cells, we automatically identified loaded entities in images of the slices, and measured the average fluorescence of these entities as a function of time. To detect individual optical events, the baseline of each trace was calculated by smoothing the trace with a high-order Hanning filter (window length, 6–7 s). We estimated the amount of noise by subtracting the baseline from the trace and measuring the standard deviation of the values of all points above the baseline. We then divided the trace by this noise level to normalize it, and considered the threshold of 1 unit below the baseline. Five action potentials were usually necessary to produce a calcium transient of this magnitude. Event times were marked at the local minima of the trace that occurred below the threshold level (Fig. 1c).

To identify peaks of synchronous activity that included more cells than expected by chance, we used interval reshuffling (randomly reordering of intervals between events for each cell) to create sets of surrogate event sequences[12]. Reshuffling was carried out 1,000 times for each movie, and a surrogate histogram was constructed for each reshuffling. The threshold corresponding to a significance level of $P < 0.05$ was estimated as the number of coactive cells exceeded in a single frame in only 5% of these histograms. We then examined each peak that was significant at $P < 0.05$, and manually rejected traces where noise was erroneously detected as an event. Peaks of synchronous activity that remained significant were selected for further analysis. For each peak of synchrony, we sought to determine whether the arrangement of cells involved could be classified into one of three spatial patterns (clusters, layers or columns) with confidence. We characterized each pattern of coactive cells by three measurements: the average distance between cell locations and their centroid, the average length of the projections of these distances in the direction parallel to the pia, and the average length of the projections in the direction perpendicular to the pia. For each pattern, we created 1,000 surrogate arrangements of cells using Monte Carlo simulations, choosing the same number of cells at random from the slice each time. All three measurements were made for each of the surrogate patterns, and the significance of the spatial arrangement was determined by directly comparing the resulting distributions with the original measurements. If distance projections were significantly small ($P < 0.05$) only in the direction parallel or perpendicular to the pia, the pattern was classified as a column or a layer, respectively. If the unprojected distances were significantly small, the pattern was classified as a cluster.

Received 16 December 2002; accepted 25 March 2003; doi:10.1038/nature01614.

1. Mountcastle, V. B. *Perceptual Neuroscience: The Cerebral Cortex* (Harvard Univ. Press, Cambridge, Massachusetts, 1998).
2. Hubel, D. H. & Wiesel, T. N. Functional architecture of the macaque monkey visual cortex. *Proc. R. Soc. Lond. B* **198,** 1–59 (1977).
3. Lorente de Nó, R. Analysis of the activity of the chains of internuncial neurons. *J. Neurophysiol.* **1,** 207–244 (1938).
4. Gilbert, C. & Wiesel, T. N. Morphology and intracortical projections of functionally characterised neurons in the cat visual cortex. *Nature* **280,** 120–125 (1979).
5. Douglas, R. J. & Martin, K. A. C. in *The Synaptic Organization of the Brain* (ed. Shepherd, G. M.) 459–511 (Oxford Univ. Press, Oxford, 1998).
6. Somogyi, P., Tamas, G., Lujan, R. & Buhl, E. Salient features of synaptic organisation in the cerebral cortex. *Brain Res. Brain Res. Rev.* **26,** 113–135 (1998).
7. Llinás, R. *I of the Vortex: From Neurons to Self* (MIT Press, Cambridge, Massachusetts, 2002).
8. Creutzfeldt, O. *Cortex Cerebri* (Oxford Univ. Press, Oxford, 1995).
9. Steriade, M., Contreras, D., Curro, D. R. & Nunez, A. The slow (<1 Hz) oscillation in reticular thalamic and thalamocortical neurons: scenario of sleep rhythm generation in interacting thalamic and neocortical networks. *J. Neurosci.* **13,** 3284–3299 (1993).
10. Tsodyks, M., Kenet, T., Grinvald, A. & Arieli, A. Linking spontaneous activity of single cortical neurons and the underlying functional architecture. *Science* **286,** 1943–1946 (1999).
11. Sanchez-Vives, M. & McCormick, D. Cellular and network mechanisms of rhythmic recurrent activity in neocortex. *Nature Neurosci.* **3,** 1027–1034 (2000).
12. Mao, B. Q., Hamzei-Sichani, F., Aronov, D., Froemke, R. C. & Yuste, R. Dynamics of spontaneous activity in neocortical slices. *Neuron* **32,** 883–898 (2001).
13. Wilson, C. J. & Groves, P. M. Spontaneous firing patterns of identified spiny neurons in the rat neostriatum. *Brain Res.* **220,** 67–80 (1981).
14. Cowan, R. L. & Wilson, C. J. Spontaneous firing patterns and axonal projections of single corticostriatal neurons in the rat medial agranular cortex. *J. Neurophysiol.* **71,** 17–32 (1994).
15. Steriade, M., Nuñez, A. & Amzica, F. A novel slow (~1 Hz) oscillation of neocortical neurons *in vivo*: depolarizing and hyperpolarizing components. *J. Neurosci.* **13,** 3252–3265 (1993).
16. Anderson, J., Lampl, I., Reichova, I., Carandini, M. & Ferster, D. Stimulus dependence of two-state fluctuations of membrane potential in cat visual cortex. *Nature Neurosci.* **3,** 617–621 (2000).
17. Fuster, J. M. The prefrontal cortex and its relation to behavior. *Prog. Brain Res.* **87,** 201–211 (1991).
18. Goldman-Rakic, P. S. Cellular basis of working memory. *Neuron* **14,** 477–485 (1995).
19. Durstewitz, D., Seamans, J. K. & Sejnowski, T. J. Neurocomputational models of working memory. *Nature Neurosci.* **3** suppl., 1184–1191 (2000).
20. Wang, X. J. Synaptic reverberation underlying mnemonic persistent activity. *Trends Neurosci.* **24,** 455–463 (2001).
21. Seung, H. S., Lee, D. D., Reis, B. Y. & Tank, D. W. Stability of the memory of eye position in a recurrent network of conductance-based model neurons. *Neuron* **26,** 259–271 (2000).
22. Hopfield, J. J. Neural networks and physical systems with emergent collective computational abilities. *Proc. Natl Acad. Sci. USA* **79,** 2554–2558 (1982).
23. Badea, T., Goldberg, J., Mao, B. Q. & Yuste, R. Calcium imaging of epileptiform events with single-cell resolution. *J. Neurobiol.* **48,** 215–227 (2001).
24. Shu, Y., Hasenstaub, A. & McCormick, D. A. Turning on and off recurrent balanced cortical activity. *Nature* **423,** 288–293 (2003).
25. Constantinidis, C., Franowicz, M. & Goldman-Rakic, P. Coding specificity in cortical microcircuits: a multiple-electrode analysis of primate prefrontal cortex. *J. Neurosci.* **21,** 3646–3655 (2001).
26. Ben-Yishai, R., Lev Bar-Or, R. & Sompolinsky, H. Orientation tuning by recurrent neural networks in visual cortex. *Proc. Natl Acad. Sci. USA* **92,** 3844–3848 (1995).
27. Hebb, D. O. *The Organization of Behaviour* (Wiley, New York, 1949).
28. Majewska, A., Yiu, G. & Yuste, R. A custom-made two-photon microscope and deconvolution system. *Pflugers Arch.* **441,** 398–409 (2000).

Supplementary Information accompanies the paper on **www.nature.com/nature**.

Acknowledgements We thank D. McCormick for advice as well as J. Hopfield and members of our laboratory for comments. Supported by NEI, NINDS, FRM, the Human Frontier Science Program, the New York STAR Center for High Resolution Imaging of Functional Neural Circuits and the John Merck Fund.

Competing interests statement The authors declare that they have no competing financial interests.

Correspondence and requests for materials should be addressed to R.C. (rcossart@biology.columbia.edu).

Turning on and off recurrent balanced cortical activity

Yousheng Shu, Andrea Hasenstaub & David A. McCormick

Department of Neurobiology, Yale University School of Medicine, 333 Cedar Street, New Haven, Connecticut 06510, USA

The vast majority of synaptic connections onto neurons in the cerebral cortex arise from other cortical neurons, both excitatory and inhibitory, forming local and distant 'recurrent' networks. Although this is a basic theme of cortical organization, its study has been limited largely to theoretical investigations, which predict that local recurrent networks show a proportionality or balance between recurrent excitation and inhibition, allowing the generation of stable periods of activity[1–5]. This recurrent activity might underlie such diverse operations as short-term memory[4,6,7], the modulation of neuronal excitability with

